LAWRENCE
LIVERMORE
NATIONAL
LABORATORY

LLNL-CONF-457153

Advances in Understanding Tokamak Edge/Scrape-Off Layer Transport

T. D. Rognlien, K. Bodi, R. H. Cohen, A. M. Dimits, M. A. Dorf, M. R. Dorr, S. I. Krasheninnikov, S. K. Nam, D. D. Ryutov, M. V. Umansky, X. Q. Xu

September 27, 2010

IAEA Fusion Energy Conference
Daejeon, South Korea
October 11, 2010 through October 16, 2010

Disclaimer

This document was prepared as an account of work sponsored by an agency of the United States government. Neither the United States government nor Lawrence Livermore National Security, LLC, nor any of their employees makes any warranty, expressed or implied, or assumes any legal liability or responsibility for the accuracy, completeness, or usefulness of any information, apparatus, product, or process disclosed, or represents that its use would not infringe privately owned rights. Reference herein to any specific commercial product, process, or service by trade name, trademark, manufacturer, or otherwise does not necessarily constitute or imply its endorsement, recommendation, or favoring by the United States government or Lawrence Livermore National Security, LLC. The views and opinions of authors expressed herein do not necessarily state or reflect those of the United States government or Lawrence Livermore National Security, LLC, and shall not be used for advertising or product endorsement purposes.

Advances in Understanding Tokamak Edge/Scrape-Off Layer Transport

T.D. Rognlien 1), K. Bodi 2), R.H. Cohen 1), A.M. Dimits 1), M.A. Dorf 1), M.R, Dorr 1), S.I. Krasheninnikov 2), S.K. Nam 1), D.D. Ryutov 1), M.V. Umansky 1), and X.Q. Xu 1)

1) Lawrence Livermore National Lab, Livermore, CA 94551 USA
2) University of California at San Diego, La Jolla, CA 92093 USA

e-mail: trognlien@llnl.gov

Abstract. Recent results are presented of plasmas transport phenomena in the edge region of tokamak devices. Fluid transport modeling results using UEDGE are given for plasma-wall interaction on the upper wall of ITER and for neutral particle fueling in DIII-D. Results for kinetic transport modeling with TEMPEST and COGENT include the combined effects of collisions and anomalous radial transport, geodesic acoustic mode damping, and collision particle loss over a confining potential barrier. Analytic theory of the edge-relevant gyrokinetic equation is presented, as is an analysis of prompt particle loss from drift orbits in the snowflake divertor.

1. Introduction

The edge/scrape-off layer (SOL) plays a number of key roles in fusion devices. Examples include: the edge/SOL controls the distribution of plasma particles and power exhausted to material surfaces, thus controlling the critical peak heat flux, and for transient events, the peak surface temperature that scales as energy/(time)$^{1/2}$. The plasma pressure at the boundary between the core plasma and this region is believed to strongly influence the energy confinement of the core plasma. The SOL helps regular particle fueling from ion recycling or gas puffing, and also acts as a shield to buffer the core plasma from the intrusion of sputtered impurities, which in the SOL can served the beneficial role of radiating localized exhaust power. Progress made in understanding a number of these issues is presented, first from fluid equation description and then from kinetic descriptions. The effect of plasma turbulence is included via anomalous diffusion and convection.

The paper is organized as follows: The advances in fluid modeling are described in Sec. 2, including particle fueling, far-SOL transport, and cross-field drifts. Contributions to kinetic edge simulation and theory are presented in Sec. 3. The conclusions are given in Sec. 4.

2. Fluid Modeling

Two issues of importance for next step devices such as ITER are first, plasma-wall interactions in regions close to a second magnetic X-point using an intermittent, between-ELM particle convection model, and second, pedestal density response and rebuilding during the ELM cycle to understand the role of neutrals from recycled ions ejected into the SOL from the ELM

Far-SOL upper-wall interactions for ITER: The impact of time-dependent (intermittent) convective or "blob" transport on plasma particle and heat fluxes to the first wall is investigated by extending the computation domain beyond the secondary separatrix of a nominally single-null divertor using the UEDGE transport code. This mesh extension technique is described elsewhere [1], where the convective transport was only represented in a time-averaged model. Here the blob transport is represented by a convective particle velocity that periodic train of pulses with a peak value 10 times the average of 60 m/sec near the wall and a duty factor of 0.1; the blob period is 0.5 ms, thus injecting plasma beyond the secondary separatrix and allowing direct contact with the upper wall along magnetic field lines. Without plasma convective transport (only diffusion with $D = 0.3$, $\chi = 1$ m^2/s), a tenuous plasma exists at the upper wall. However, with the present 2D time-dependent convection model shows

that a substantial flux of particles then recycles on the upper wall, but even though the plasma and especially neutral densities are strongly modulated, the peak heat flux remains low because dense, detached plasma is quickly formed on the upper wall from the large recycling particle flux as shown in Fig. 1 shortly after the peak of the outward convective radial

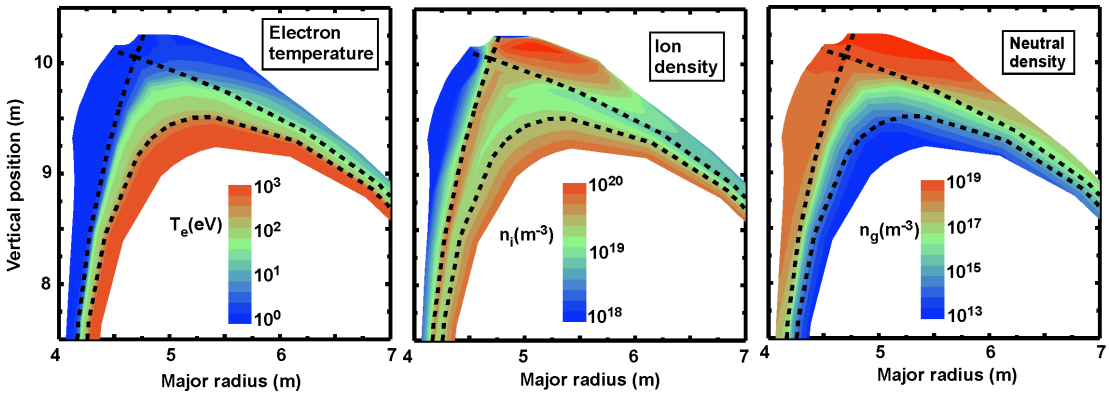

FIG. 1. Contours of parameters near ITER's upper wall when 2D convective transport is included. Dashed lines are primary (inner) and secondary (outer) separatrices.

velocity. On the other hand, it is anticipated that using a similar model for ELMs, the heat flux to the top wall can be substantial, which is the subject of ongoing work. Extensions needed beyond the present 2D model are 3D blob and ELM models where peak localized heat fluxes will be higher.

***Particle edge fueling during DIII-D ELM cycle*:** The fueling of the pedestal from neutrals generated by recycled ions is an important issue for future devices, and time-dependent transport modeling can help identify key processes and timescales. Specifically, UEDGE is used to study particle fueling for DIII-D over a sequence of a number of ELM cycles in the midst of a long regular ELM sequence. Here the wall, divertor, and pumps are assumed to have come into particle equilibrium when averaged over a complete ELM cycle, as evidenced by the nearly constant discharge conditions. Between ELMs, the radial transport coefficients are taken from an interpretive analysis without a pinch term (varying $D \sim 0.02$, $\chi \sim 0.5$ m^2/s in pedestal, $D = 0.3$, $\chi = 1$ m^2/s in SOL), and the ELM itself is represented by large transport ($D = 5$, $\chi = 10$ m^2/s) on the low B-filed side for a 200 μs period. In the inter-ELM period, a pinch velocity could have been combined with a larger D value for the same steady-state flux, but the option is not examined here. For particles, the only net source of particles corresponds to an ion flux at the core boundary corresponding to the neutral beam fueling in the core of 60 Amps for DIII-D discharge 118898 at 3500 ms. The divertor and wall recycling coefficients are unity and there is no pumping.

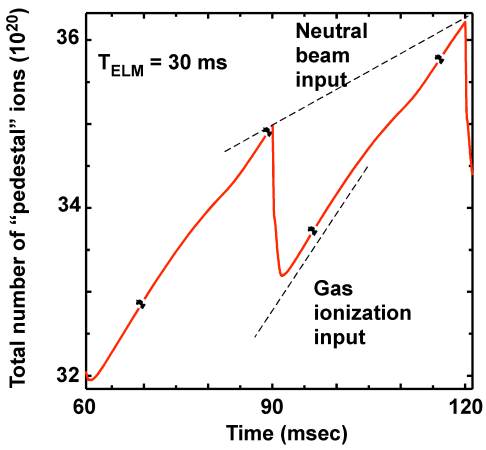

FIG. 2. Total number of ions in the pedestal region during 2 ELM cycles

The resulting total number of particle in the pedestal region defined by normalized poloidal flux from 0.8 to 1.0 is shown in Fig. 2 for two ELM periods with each ELM corresponding to the steep drop in the pedestal density. Note that for this case, the neutral ionization provides the dominant rise in pedestal density compared to the core ion flux from neutral beam input. Though qualitatively consistent with the data, a discrepancy is the apparent nearly linear rise of the pedestal density over the ELM period here compared

to profile data that indicates a rapid rise followed by saturation [2]. Such a variation could be caused by temporal changes in the transport coefficients or depletion of the neutrals (which should be included here). The SOL plasma changes substantially over the cycle to first shield, and then promote, neutral fueling from recycled ions owing to growing ion/neutral temperatures. A prominent feature in the divertor region is the substantial rise in plasma density in the private flux region following the ELM with a slow reduction before the next ELM.

3. Kinetic Modeling

Kinetic modeling of the edge/SOL is performed with two 4D (2r,2v) continuum codes, TEMPEST and COGENT, as part of our Edge Simulation Laboratory work. The more mature TEMPEST has simulated the effect of collisions and a spatial diffusion coefficient to represent the effect of turbulence, and the synergistic effect of the neoclassical and anomalous transport is studied. Development of COGENT is illustrated by studies of geodesic acoustic mode (GAM) damping and particle loss from collisional scattering over a potential barrier.

Anomalous radial edge transport for kinetic codes: One of the long-standing issues of edge plasma transport simulation is the applicability of fluid models for parallel heat transport. For typical plasma parameters in the scrape off layer (SOL) of fusion devices, the ratio of coulomb collision mean free path to the magnetic connection length in the SOL is of the order of 0.1. Even though it is smaller than unity it is still too large for Spitzer-Harm model of heat conduction to be valid. In addition, sharp transitions between the plasma and material surface, and between the closed and open magnetic field line regions, also raise the doubt in the applicability of fluid models, which are widely used for the assessment of plasma-wall interactions in both current devices and ITER. To go beyond fluid approximation in transport study in edge plasma one needs to consider two dimensions in both configuration and velocity spaces (2D2V). However, this is very complex task and so far only 1D2V models of edge plasma kinetic problem have been studied (*e.g.* see Ref. [3,4]) and the references therein). Here we report our preliminary results on 2D2V kinetic modeling of tokamak plasmas with the TEMPEST code. For the cross-field plasma transport, we use convective-diffusion model for the flux, Γ_ψ, across the magnetic flux surfaces, ψ,

$$\Gamma_\psi = U_f f - D_f \nabla_\psi f\,, \tag{1}$$

where the convection and diffusion coefficients are

$$U_f = \frac{2}{3}\left(\chi - \frac{7}{2}D\right)\nabla_\psi \ell n(n) + \nabla_\psi \ell n(T)\,, \text{ and } \; D_f = \frac{2}{3}\left(\chi - \frac{7}{2}D\right) + \frac{2}{3}\left(\frac{\vec{v}}{v_t}\right)^2 D. \tag{2}$$

Here χ and D are the velocity-space-averaged cross-field heat diffusivity and particle diffusion coefficients corresponding to the Maxwellian distribution function, and $v_t = (T/m)^{1/2}$ is the mean thermal velocity. Note that the kinetic D_f is velocity dependent. The kinetic equation is then solved for the particle distribution f,

$$\frac{\partial f}{\partial t} + v_\parallel \cdot \nabla_\parallel f + \vec{v}_{dr} \cdot \nabla_\perp f + eE_\parallel \frac{\partial f}{\partial v_\parallel} + \nabla_\psi \cdot \left\{\Gamma_\psi \vec{e}_\psi\right\} = C + S, \tag{3}$$

where f is a function of ψ, poloidal angle θ, particle energy E, and magnetic moment μ, and $\vec{e}_\psi$ is the unit vector perpendicular to the magnetic surface ψ. Further, C and S are the collision and source terms. For a toroidal annulus geometry specifying Maxwellian distribution function on the boundaries of the domain in ψ coordinate and using, as a first step, Krook collision operator to maintain the distribution close to Maxwellian. The impact of

anomalous radial diffusion ion density and temperature in this kinetic model can be seen from Fig. 3, where initial exponential profiles are subjected to strong collisions and radial diffusion.

A second result from the anomalous radial diffusion model in TEMPEST is obtained in divertor geometry where D_f is a constant. We steady solutions of neoclassical transport together with model anomalous transport [5]. A series of such simulations are conducted to investigate the transition of midplane pedestal heat flux and flow from the neoclassical to turbulent limit and the transition of divertor heat flux and flow from kinetic to fluid regime via a density-scan and an anomalous transport scan. TEMPEST simulations include turbulent transport decorrelation of particle drift orbits and thus localization, much as collisions do. Consequently, large turbulent transport leads to the reduction of non-Maxwellian features in the particle distribution function. It is also found the transition of parallel heat flux and flow at the entrance of divertor plates from fluid to kinetic regime, leading to a modified relationship of flux-limited heat flux. Even for an absorbed divertor plate boundary condition, a non-half-Maxwellian is found due to the substantial collision for slow particles. In Fig. 4, we show the steady-state parallel ion heat flux on radial-poloidal plane for the anomalous diffusion coefficient $D = 1$ m^2/s, and a scan of the heat flux via anomalous diffusion coefficient D calculated by TEMPEST for the DIII-D geometry.

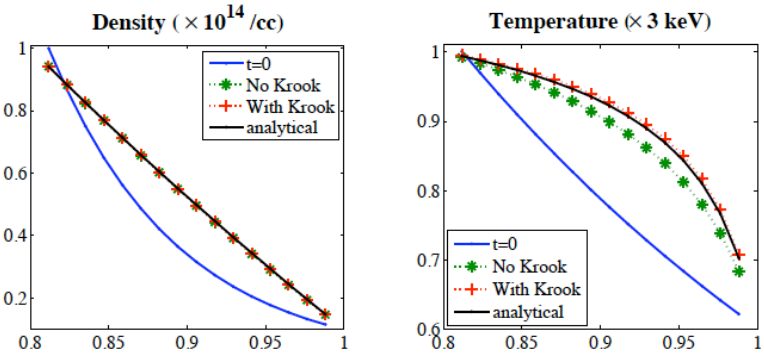

FIG. 3. Effect of collisions on spatial distribution of density and temperature. Curved temperature profile is caused by the contribution into energy flux of both convective and heat diffusive terms.

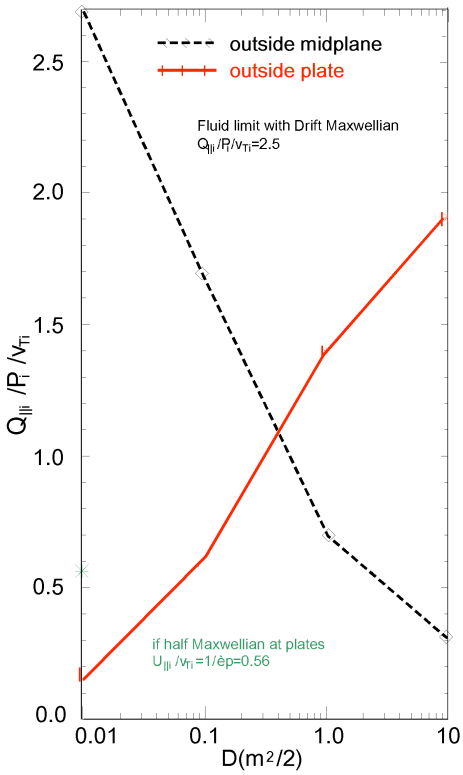

FIG. 4. Parallel ion heat flux in radial-poloidal plane and the scan of the heat flux via anomalous diffusion coefficient D calculated by TEMPEST for the DIII-D geometry.

The mid-plane plasma follows neoclassical dynamics and the ion parallel heat flux decreases as D increases because the large D flattens the plasma profiles, leading to smaller parallel flux as neoclassical theory predicts. While at the divertor plate, the endloss and collision dominates the dynamics. The ion parallel heat flux decreases as D decreases. The theoretical prediction is a half Maxwellian ion distribution at the divertor entrance, however, TEMPEST simulations yield an ion parallel heat flux smaller than that calculated from the half-Maxwellian due to the substantial collision for slow particles and particle drift orbit effects.

Development of kinetic COGENT: COGENT is a code currently in development, utilizing a 4th-order conservative finite volume numerical scheme to implement a conservative formulation of the gyrokinetic equation (presently, that of Hahm [6]), combined with a flux

limiter that suppresses oscillations near sharp-gradient regions of the distribution function. Verification tests have been performed to illustrate the correctness and power of the new algorithm. These include basic advection tests, trapped-particle orbit tests, evolution of steep gradient profiles under the influence of neoclassical orbits with and without a toroidal limiter, and simulations of one-dimensional acoustic waves and two-dimensional geodesic acoustic modes (GAMs), and initial tests of a simple collision operator.

GAM studies with COGENT: In particular, our setup for GAMs is similar to that reported previously [7]: doubly periodic boundary conditions, with radially constant metric coefficients; and an initial condition consisting of a purely radially varying sinusoidal density perturbation, with a Boltzmann electron response of the form $n_e = n_0 \exp(e\phi/T_e)/\langle \exp(e\phi/T_e)\rangle$ where $\langle\ \rangle$ denotes a flux-surface average and n_0 is the volume-averaged ion density. The parameters are the same as Ref. [7]. We compare the numerically obtained damping rates and real frequencies with those which we obtain analytically following the prescription Gao *et al*. [8], as well as with the other codes included in the study in Ref. [9]. The results for the damping rate are shown in Fig. 5. As can be seen, the COGENT results at both $T_e/T_i = 0$ and $T_e/T_i = 1$ agree quite well with theory, seemingly better than the other codes (which were all run for $T_e/T_i = 1$). Since obtaining these results we have learned that the XGC-1 results retained only the flux-surface-averaged component of ϕ, which renders the calculation equivalent to setting $T_e = 0$ [10]. The discrepancy with GYRO results may be the result of a different procedure to deduce damping rates. Comparably good agreement is obtained for the real frequency.

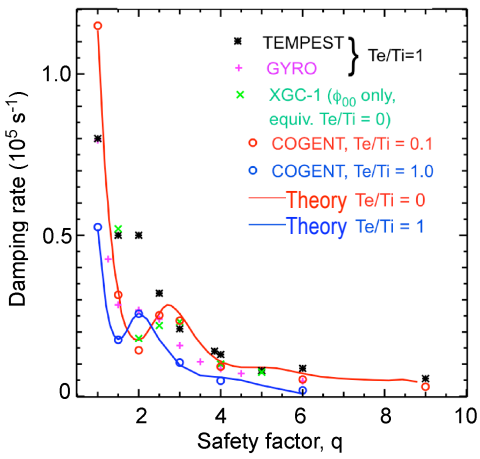

FIG. 5. Damping rate for GAMs vs safety factor, simulation (points) and theory (lines).

Collisions in COGENT: We have implemented an initial collision model in COGENT, *i.e.*, a model for the kinetic collision operator C in Eq. 3. A model collision operator providing drag and diffusion in the parallel velocity space,

$$C(f) = \nu_c \partial_{v_\parallel}\left[v_\parallel f + (T/m)\partial_{v_\parallel} f\right] \qquad (4)$$

is implemented, and initial testing results are presented here. Here ν_c is the collision frequency. Excellent agreement with an analytical theory was observed for the Pastukov-type test problem, where particles confined along the magnetic field direction by a square electrostatic potential well become untrapped due to the re-population of the high-parallel-velocity distribution function by collisions (Fig. 6). The figure shows the decay of particle distribution function f due to the parallel loss over a potential barrier. The results correspond to the case of weak collisions, where the collision frequency much less than the parallel bounce frequency. Here, a fitting parameter is used to position the vertical position of the dashed line. Implementation of other model collision operators including the Lorentz

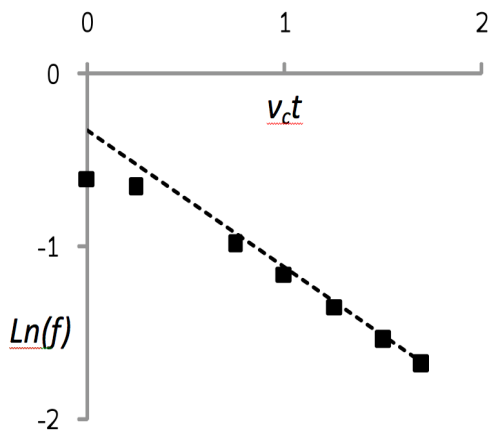

FIG. 6. COGENT simulations (dots) of the decay of f versus time in an electrostatic well with the particle collision model of Eq. 4. The asymptotic decay obtained analytically is given by the dashed line.

operator, the linearized collision operator, and the full non-linear Landau operator is currently underway.

Also underway is the upgrade of COGENT to include divertor geometry. This is based on arbitrarily mapped multi-block grid technology, which will also be a key mechanism for handling magnetic shear in our planned 5D extension (adding the toroidal dimension).

Gyrokinetic theory: We have development valid electromagnetic gyrokinetic equation sets for large edge perturbations as well as methods for implementing most of the terms that have not previously been implemented. We have generalized our previous extended-ordering gyrokinetic derivation [11] to include toroidal geometry and electromagnetic perturbations. The results, at least for edge and transport-barrier-like conditions where the radial plasma profile scale is much shorter than that of the magnetic field variation, are essentially the same as those of derivations using "standard" gyrokinetic orderings [12], but our derivation shows that these equations are valid even if the potential perturbations are of order the thermal level, provided that any $\boldsymbol{E}\times\boldsymbol{B}$ drifts are much slower than the sound speed. An additional low-β subsidiary ordering simplifies the equations further (at second order in the gyrokinetic parameter), while retaining standard low-β electromagnetic physics (both linear and nonlinear).

Methods for implementing the second-order terms in this equations of motion in this set have been developed, based on straightforward extensions of the methods that are in use for the first-order terms in core gyrokinetic codes. A practical direct finite-element discretization of the evolving gyrokinetic Poisson-equation operator has also been developed, which is an extension of the finite-element method used by Mischenko *et al.* [13], to include the remaining second order terms.

In order to account for the possibility of large self consistent $\boldsymbol{E}\times\boldsymbol{B}$ drifts, a gyrokinetic theory has recently been developed in an extended ordering in which the small parameter is the ratio of the $\boldsymbol{E}\times\boldsymbol{B}$ shearing rate to the gyrofrequency [14]. This allows for long wavelength $\boldsymbol{E}\times\boldsymbol{B}$ flows of order the thermal velocity, while recovering all terms in the standard and small-$\boldsymbol{E}\times\boldsymbol{B}$-flow equations under the respective subsidiary orderings. The new theory generalizes prior work [15,6] to allow for time dependence in the large long-wavelength component of the electric field, and a continuum of scales in the field components rather than just two distinct components. Additionally, new terms were found that result from the beating of the gyrophase dependences of the equilibrium and perturbed fields and which should be present even under the assumptions of the earlier works. This set of equations is much more complicated and challenging to implement than those derived in the small-$\boldsymbol{E}\times\boldsymbol{B}$-flow ordering, and further work is required to develop implementation methods for them.

Collisions are also important for the edge region, so it is important to develop a valid and practically implementable large-perturbation gyrokinetic collision operator. We have therefore surveyed and carried out needed extensions to the theory underlying such an operator. Brizard [16] had showed that because the collisional coupling between the gyrophase-independent and dependent parts of the distribution function is weak, a bilinear gyrokinetic Coulomb collision operator can be formulated in terms of the gyrophase independent part. This work resulted in a straightforward expression for the collision operator, and formed the theoretical foundation for some numerical implementations [17], but was incomplete because the action of collisions on the (non-Maxwellian) polarization (or pullback) contribution to the distribution function, which are of the same formal order as the perturbed distribution function itself [18], were neglected. We have derived a corrected bilinear Coulomb collision operator that includes the first-order pullback terms in the distribution function, and have worked out methods for implementing these terms.

Drift-orbit loss in Snowflake divertors: The behavior of the plasma in the pedestal region is affected by a variety of factors, including the velocity shear. The flow velocity, in turn, is largely controlled by the normal (to the flux surfaces) electric field. It has been noticed long ago that this field can be strongly affected by the prompt ion losses from the poloidal-B-field null point region [19,20]. The loss mechanism is determined by the slowness of the poloidal ion motion (even for the thermal ions) in the vicinity of the null point (the poloidal projection of the parallel ion velocity is small due to the smallness of the poloidal field). The poloidal velocity is especially small for the ions with the turning points situated near the null. Such ions reside for a long time near the null-point and can be moved across the separatrix (and lost) by the ∇B drift.

This mechanism is significantly amplified in the recently proposed snowflake divertor configuration [21,22], where the poloidal field has a second-order null: with both the poloidal field and its first spatial derivatives simultaneously zero. The poloidal field strength now is a quadratic function of the distance to the null-point, meaning that the poloidal field and the ion poloidal velocity are very small in the null-point region. This leads to the increase of the zone inside the separatrix affected by the prompt losses and to a significant increase of the loss rate. Therefore, one can expect that the snowflake configuration would have a higher velocity shear in the pedestal region, this lending one more control mechanism over ELMs.

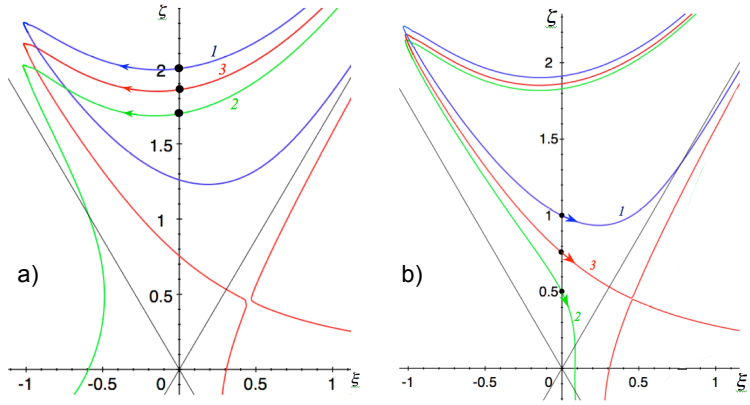

FIG. 7. Ion trajectories near a snowflake null point in normalized (R,Z) coordinates. Black straight lines – the separatrix; black dots – initial positions; arrows - initial direction; from Ref. [23]. Red trajectories separate confined and prompt-loss regions. a) Ions initially moving left [to high-B-field side] and b) ions initially moving right.

The analysis of the ion trajectories in the snowflake divertor [23] has revealed that the zone affected by the prompt loss mechanism extends by the distance $\sim a(\rho_{iP}/a)^{2/5}(a/R)^{1/5}$ above the null-point [a and R are the minor and the major radii, and ρ_{ip} is the ion gyroradius evaluated with the mid-plane poloidal field]. This distance is a few times deeper into the core plasma than for the standard X-point divertor, for which the analogous estimate reads as $a(\rho_{iP}/a)^{2/3}(a/R)^{1/3}$. Note that the energy loss is negligibly small, but as it affects only the ions, it may lead to a significant build-up of the radial field by the quasineutrality constraint [19,20]. Characteristic shape of the trajectories (projected onto poloidal plane) is shown in Fig. 7. We are now performing an analysis of the effect of collisions and radial electric field on prompt losses with a Monte-Carlo code being developed for this purpose.

4. Conclusions

Results have been presented of advanced understanding of tokamak edge plasmas through the use of fluid and kinetic simulation and theory. One fluid analysis was UEDGE transport modeling of edge/SOL plasma in ITER that includes both the SOL region beyond the secondary X-point and a time-dependent representation of between-ELM blob transport via a 2D convective model. Here the wall region near the upper X-point has substantial particle flux and recycling, but low heat flux; this result may change with a 3D blob model and for

ELMs. The second fluid transport analysis show that for DIII-D, neutral particle fueling of the pedestal can sometimes be important for density buildup between ELMs.

Kinetic transport analysis considered the combination of an anomalous radial transport model that has the flexibility to represent the commonly used diagonal transport matrix model in fluid codes. Combining anomalous radial transport with collision in a single-null divertor geometry with TEMPEST illustrated the competition between neoclassical and anomalous transport, where strong anomalous transport behaves similar to collisions in reducing non-Maxwellian features. The capabilities of the new COGENT kinetic code are illustrated by a careful comparison for GAM damping that shows good comparison to theory, clarifying the important effect of the electron-to-ion temperature ratio. An initial collision model in COGENT is found to accurately describe loss of particles from a potential trap. A new, recently published gyrokinetic theory applicable to edge conditions is summarized. The theory uses an extended ordering in which the small parameter is the ratio of the $\boldsymbol{E}\times\boldsymbol{B}$ shearing rate to the gyrofrequency, which allows for long wavelength $\boldsymbol{E}\times\boldsymbol{B}$ flows of order the thermal velocity. Finally, an analysis is presented yielding the boundary between confined and unconfined drift orbits near the magnetic separatrix in a single-null snowflake divertor configuration. Owing to the reduction of the poloidal B-field near the null point, orbit loss can extend to a wider set of particles for the snowflake compared to the standard, likely impacting the radial electric field.

Acknowledgements

Work performed for the US Department of Energy under the auspices of the Lawrence Livermore National Laboratory under contract DE-AC52-07NA27344 and by UCSD under Contract DE-FG02-04ER54739. Thanks to R. Groebner for DIII-D edge profile fits.

References

[1] ROGNLIEN, T.D., BULMER, R.H. *et al.*, J. Nucl. Mater. **363-365** (2007) 658.
[2] GROEBNER, R.J., OSBORNE, T.H. *et al.,* Nucl. Fusion **49** (2009) 045013.
[3] BATISHCHEV, O.V. *et al*., Phys. Plasma **4** (1997) 1672.
[4] TSKHAKAYA. D.D. *et al.*, Contr. Plasma Phys. **48** (2008) 89.
[5] XU, X.Q., BODI, K., COHEN, R.H. *et al.* Nucl. Fusion **50** (2010) 064003.
[6] HAHM, T.S., Phys. Plasmas **3** (1996) 4658.
[7] XU. X.Q., XIONG, Z., GAO, Z. *et al.,* Phys. Rev. Lett.
[8] GAO, Z., ITOH, K. *et al.,* Phys. Plasmas **15** (2008) 072511.
[9] XU. X.Q., BELLI, E., BODI, K. *et al.*, Nucl. Fusion **49** (2009) 065023.
[10] CHANG, C.-S., private communication (2010).
[11] DIMITS, A.M., LODESTRO, L.L., DUBIN, D.H.E., Phys. Fluids B **4** (1992) 274.
[12] BRIZARD, A.J, and HAHM, T.S., Rev. Mod. Physics **79** (2007) 421.
[13] MISCHENKO, A., KONIES, A., and HATSKY, R., Phys. Plasmas **12** (2005) 062305.
[14] DIMITS, A.M., Phys. Plasmas **17** (2010) 055901.
[15] BRIZARD, A.J. Phys. Plasmas **2**, 459 (1995)
[16] BRIZARD, A.J., Phys. Plasmas **11** (2004) 4429.
[17] XIONG, Z., COHEN, R.H. *et al.*, J. Comp. Phys. **227** (2008) 7192.
[18] XU, X.Q., ROSENBLUTH, M.N., Phys. Fluids B **3** (1991) 627.
[19] CHANKIN, A.V., MCCRACKEN, Nucl. Fusion **33** (1993) 1459.
[20] CHANG, C.-S., KUE, S., WEITZNER, H., Phys. Plasmas **9** (2009) 025007.
[21] RYUTOV, D.D., Phys. Plasmas **14** (2007) 064502.
[22] RYUTOV, D.D., COHEN, R.H. *et al.,* Phys. Plasmas **15** (2008) 092501.
[23] RYUTOV, D.D., UMANSKY. M.V., Phys. Plasmas **17** (2009) 014501.